QUANTUM SENSING

Atomic-scale quantum sensing based on the ultrafast coherence of an H_2 molecule in an STM cavity

Likun Wang[1], Yunpeng Xia[1], W. Ho[1,2]*

A scanning tunneling microscope (STM) combined with a pump-probe femtosecond terahertz (THz) laser can enable coherence measurements of single molecules. We report THz pump-probe measurements that demonstrate quantum sensing based on a hydrogen (H_2) molecule in the cavity created with an STM tip near a surface. Atomic-scale spatial and femtosecond temporal resolutions were obtained from this quantum coherence. The H_2 acts as a two-level system, with its coherent superposition exhibiting extreme sensitivity to the applied electric field and the underlying atomic composition of the copper nitride (Cu_2N) monolayer islands grown on a Cu(100) surface. We acquired time-resolved images of THz rectification of H_2 over Cu_2N islands for variable pump-probe delay times to visualize the heterogeneity of the chemical environment at sub-angstrom scale.

Quantum sensing and quantum computing, together with other quantum processes, have shown advantages over their classical counterparts (*1*, *2*). Unlike quantum computing, which pursues the long decoherence time in a robust quantum system such as an isolated qubit, quantum sensing capitalizes on the weakness of a quantum system for its high sensitivity to the external environment. Although nitrogen vacancy (NV) centers (*3*–*6*), trapped ions (*7*), and single-electron transistors (*8*, *9*) have been used as quantum sensors, atomic-scale spatial resolution has been impeded by the large size of existing sensors or the limitations of experimental techniques.

The scanning tunneling microscope (STM) offers atomic-scale measurement and control of molecular systems in a surrounding environment that can be characterized by imaging (*10*). A molecular quantum dot has been attached to the STM tip to measure the surface electric potential (*11*). Electron spin resonance sensors based on single magnetic atom–functionalized tips have probed the local magnetic fields produced by atomic and molecular spins (*12*–*16*). The combination of STM and femtosecond lasers has probed the temporal dynamics of molecular motions in the STM cavity with atomic-scale spatial resolution far below the diffraction limit (*17*–*19*).

Here, we studied single H_2 molecules in the cavity defined by the Ag tip and a Cu_2N island grown on the Cu(100) surface using a femtosecond laser, corresponding to terahertz (THz) frequencies, together with a low-temperature STM. By performing THz rectification spectroscopy (TRS) and THz pump-probe measurements, we demonstrate the sensitivity of the coherence of a single H_2 molecule to its immediate environment. The THz pulses in the STM cavity can couple two low-lying states of H_2 in a double-well potential and create a superposition that oscillates periodically with a frequency corresponding to the energy separation of the two states. The damping of this coherent oscillation provides a measure of the decoherence time from the interaction of the two-level system (TLS) with its surrounding environment.

Experiments were performed in a home-built ultrahigh-vacuum (UHV) STM at a base temperature of 9.0 K and with silver (Ag) tips. A femtosecond Ti:sapphire laser with 1-GHz repetition rate was used to generate THz pulses from a plasmonic photoconductive antenna (*20*). The THz pulses were aligned and focused into the cavity through flat silver mirrors and aspheric Tsurupica lenses. The experimental approach is shown schematically in Fig. 1A, and additional details are described in the supplementary materials (figs. S1 and S2).

Hydrogen molecules adsorb on a variety of materials, including metal surfaces (*21*), insulating layers (*22*–*26*), and single molecules (*27*, *28*). To describe a H_2 molecule in the tunnel junction, a TLS in a double-well potential has been widely adopted (*29*, *30*) in which the H_2 molecule switches between two different adsorption configurations (*31*) (Fig. 1B). The population change from the predominant lower state $|a\rangle$ to upper state $|b\rangle$ can be greatly enhanced when the tunneling electrons have sufficient energy to excite H_2 external vibrational or rotational states (*30*) lying above the central barrier of the double-well potential.

With a H_2 molecule weakly trapped inside the STM cavity, the spatial resolution in constant-current topography can be greatly enhanced (*22*). A topographic image of an incommensurate Cu_2N island grown on Cu(100) (*32*) is shown in Fig. 1C, with a close-up image in Fig. 1D. By performing inelastic electron tunneling spectroscopy (IETS) measurements over different sites of the Cu_2N island (Fig. 1E), we confirmed the presence of an H_2 molecule in the cavity (*25*–*27*). The $\nu = 0 \rightarrow 1$ excitation of the external vibration at ±20 mV and $j = 0 \rightarrow 2$ (para-hydrogen) rotational excitation at ±43 mV did not show resolvable differences for the three high-symmetry positions over Cu_2N.

The spatial variations of the charge distribution on the heteroatomic Cu_2N surface (*33*) were expected to induce a dipole moment in the adsorbed H_2 molecules. Femtosecond THz laser pulses irradiating the STM cavity can excite the TLS, change its population, and facilitate tunneling of H_2 between the two states. To extract the population change from the tunneling current induced by THz irradiation, we implemented atomic-scale rectification spectroscopy, which was initially demonstrated in the microwave frequency range (*34*, *35*). The calibration of the absolute rectification current is shown in fig. S3. A peak voltage of 4.2 mV was derived from THz irradiation by comparing the peak width of IETS and TRS measurements. Further discussion on this weak THz field is given in the supplementary materials (fig. S4). Single-beam TRS shows unchanged vibrational and rotational excitation energies (Fig. 1F) for the same tip-substrate separation and substrate positions as IETS in Fig. 1E. However, the spectral line shapes in Fig. 1, E and F, substantially differ because of population change in the H_2 TLS induced by the THz pulses.

To monitor the temporal evolution of the THz-induced population change, we conducted THz pump-probe measurements over H_2 trapped between the STM tip and the Cu_2N surface. The rectification current was recorded as a function of the time delay τ between two nearly identical THz beams (Fig. 2A). Coherent oscillations with temporal decay and beating were clearly resolved with the tip positioned over different positions of the Cu_2N island. At each of the three high-symmetry positions, a strong peak appeared in the fast Fourier transform (FFT) that corresponded to the main oscillation in the time domain. Additionally, the beating in each delay scan led to satellite peaks in the frequency domain. Similar oscillation was also seen in the spectral intensity of TRS for different delay times, as shown in fig. S5. Additional details and analyses are described in the supplementary materials.

The coherent oscillations of H_2 were sensitive to the position of the tip over the Cu_2N island (Fig. 2A). The description of the Cu_2N lattice is given in fig. S6. No substantial difference in the vibrational and rotational excitation energies could be resolved by IETS and single-beam TRS for the STM tip over the three lateral positions of the Cu_2N layer. In contrast, the THz pump-probe measurements revealed largely distinct frequencies for the three positions (Fig. 2B). For example, an

[1]Department of Physics and Astronomy, University of California, Irvine, CA 92697, USA. [2]Department of Chemistry, University of California, Irvine, CA 92697, USA.
*Corresponding author. Email: wilsonho@uci.edu

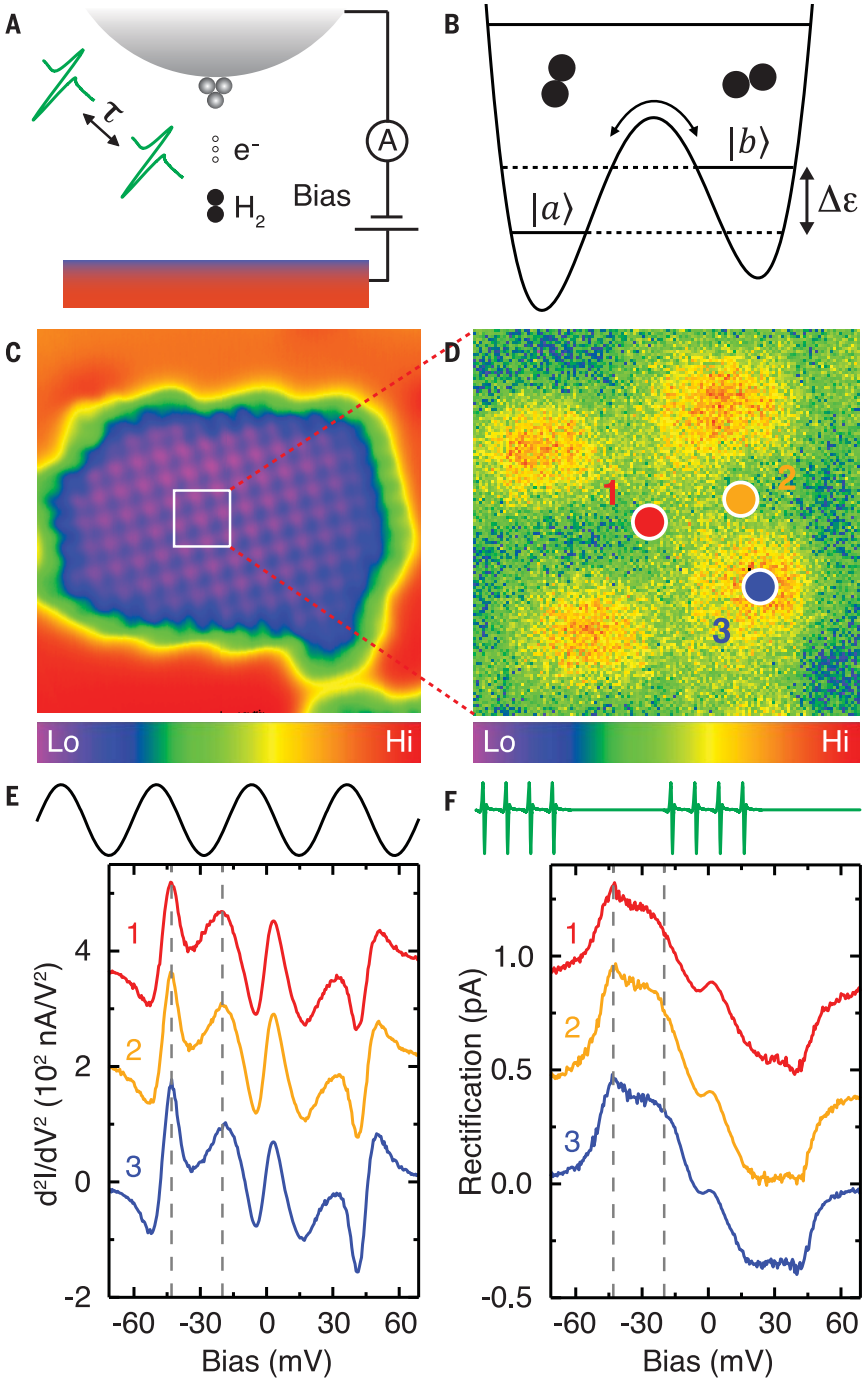

Fig. 1. IETS and TRS of H_2 over different sites of Cu_2N. (**A**) Schematic diagram of THz-STM experimental setup. τ is the temporal delay between the pump-probe THz pulses. (**B**) Asymmetric double-well potential of H_2 molecule in STM cavity. (**C**) Constant-current topography of Cu_2N island acquired with Ag tip; image size 62.0 Å × 62.0 Å. Scanning condition: −20 mV/0.3 nA. (**D**) Zoom-in topographic image of the Cu_2N island, 7.4 Å × 7.4 Å, with red (1), yellow (2), and blue (3) dots over the hollow, bridge, and top sites of the Cu_2N lattice, respectively. (**E**) STM-IETS measurements of H_2 molecule acquired with root-mean-square bias modulation of 3 mV at 263.03 Hz. Tip is positioned at the three different positions labeled in (D) with −20 mV/40 pA setpoint. The black curve in the upper schematic illustrates the sine-wave modulation for IETS. (**F**) TRS measurements of H_2 molecule over the three high-symmetry positions. Single beam of THz pulses is aligned into the junction with the same setpoint and chopped at the same frequency as the STM-IETS for acquiring the spectra. The green curve in the upper schematic illustrates modulation of the single THz beam for TRS. Within half of each square-wave modulation period, a pulse train of ~1.9 million THz pulses is directed into the STM cavity. Dashed lines in (E) and (F) mark the excitation energies of the external vibration and rotation at −20 mV and −43 mV, respectively. All of the spectra in (E) and (F) are offset vertically for clarity.

oscillation frequency shift of 0.11 THz was recorded from position 2 (0.26 THz) to position 3 (0.37 THz), which corresponds to a sensitivity of 58 GHz/Å in the surface plane. The frequency difference was well resolved in the FFT spectrum even though the lateral distance between positions 2 and 3 was only 1.9 Å.

The lattice mismatch between Cu_2N and Cu(100) (*32*) and the asymmetry of the STM tip could induce multiple closely related configurations of H_2 and lift the degeneracy of the TLS energy levels, which led to satellite peaks in the FFT spectrum (Fig. 2B). By fitting multiple sinusoidal functions with an exponential decay term to the coherent oscillations over each position (fig. S7), we could also extract the decoherence time T_2, as shown in the inset of Fig. 2B. Positions 1 and 3 showed similar T_2 around 45 ps, whereas position 2 exhibited a longer time of 80 ps. A set of THz pump-probe measurements with the STM tip over a series of the protrusion sites across the Cu_2N island is shown in fig. S8, illustrating the high spatial sensitivity of the coherent oscillations and surface heterogeneity. In addition, the coherent oscillation over position 1 of fig. S8A exhibited negligible beating and revealed a single peak located at 0.444 THz in the FFT spectrum (fig. S9). The full width at half-maximum (FWHM) of the peak was 4.3 GHz by fitting with a Gaussian peak. Taking the resolving power to be the separation of two peaks by the FWHM, the THz pump-probe measurements could resolve a frequency shift of 4.3 GHz or an energy of 18 μeV.

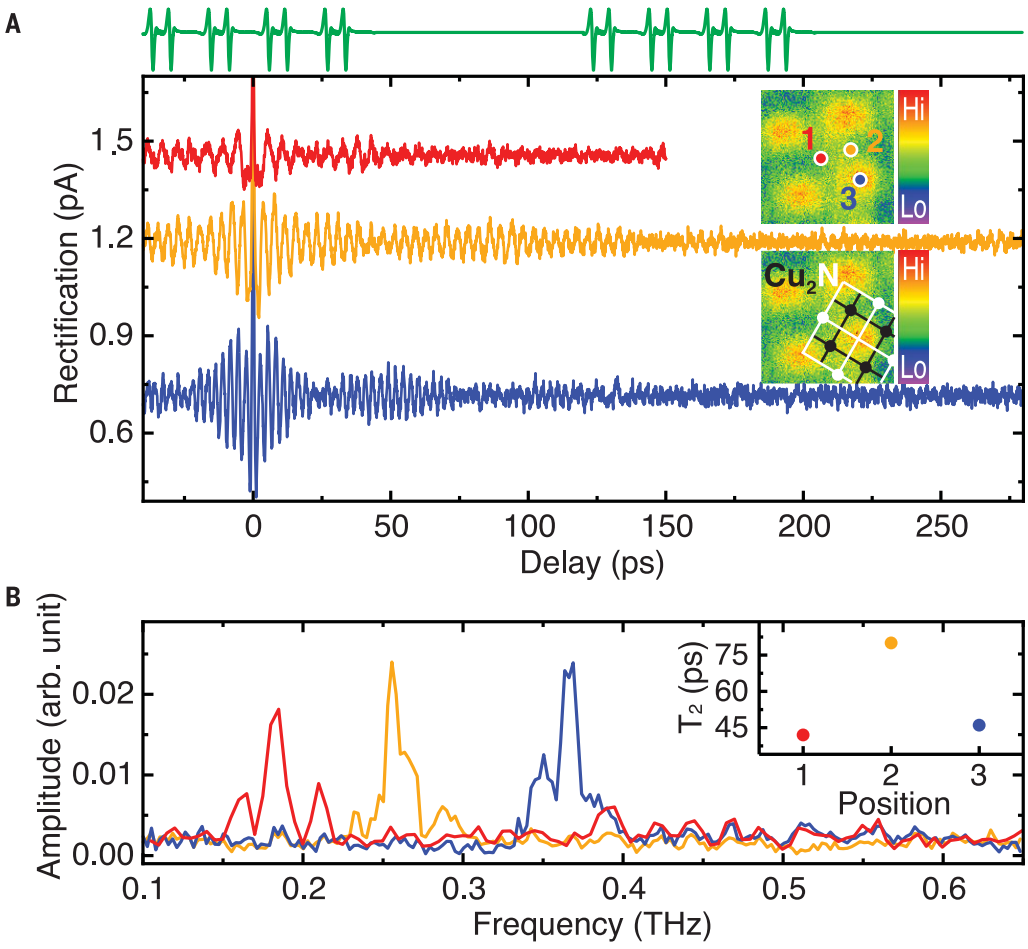

Fig. 2. THz pump-probe measurements of H_2 over different positions of Cu_2N. (**A**) Time-domain measurements of the THz rectification current through H_2 over three lateral positions. The tip is positioned over the correspondingly colored spots with the feedback setpoint −20 mV/40 pA. The feedback is then turned off and sample bias is ramped to −30 mV for the measurements. All of the spectra are offset vertically for clarity. The green curve in the upper schematic illustrates modulation of THz pump-probe beams for TRS. Within half of each square-wave modulation period, a pulse train of ~1.9 million THz pulse pairs is directed into the STM cavity. Inset: Constant-current STM topography of Cu_2N surface, 7.4 Å × 7.4 Å, showing the tip positions (1, 2, and 3) and lines connecting the Cu and N atoms in the two sublattices. (**B**) FFT results of the corresponding measurements in (A). Inset: Decoherence times extracted from fitting of the data shown in (A).

The periodic arrangement of non-neutral Cu and N atoms determines the surface chemical environment distribution of Cu_2N (*36*, *37*). When the tip was placed over the three high-symmetry positions with the same setpoint, the H_2 molecule trapped inside the cavity exhibited different dipole moments caused by the heterogeneous atomic composition of the underlying surface. As a result, the energy separation of the two levels changes, making the H_2 molecule a sensitive probe of the surface chemical environment.

The effect of intermolecular interactions from other adsorbed H_2 molecules was ruled out with the observation of a constant oscillation frequency at various H_2 concentrations (fig. S10). Unlike the IETS and single-beam TRS, which showed no resolvable position-dependent differences on the excitation energies, THz pump-probe measurements probing the TLS coherence showed an advantage in sensing changes in the molecular environment. In addition to the frequency shift, the decoherence time of the oscillations also exhibited spatial dependence at the atomic scale.

The energy difference of the TLS could also be tuned by varying the tip-substrate separation, which was controlled by adjusting the tunneling current at constant sample bias. As the tunneling current increased from 0.02 to 0.2 nA, the tip moved toward the surface by ~1 Å. A series of THz pump-probe measurements at different tip-substrate separations (Fig. 3A) showed that as the tip approached the substrate, the coherent oscillation gradually became weaker. A color map of the measurements (fig. S11B) shows changes in the oscillation period and amplitude as a function of tip-substrate separation.

The frequency from the FFT exponentially increased as the tip-substrate separation decreased (Fig. 3B). A frequency sensitivity of 0.19 THz/Å in the normal direction (tunneling gap) was determined. Both the oscillation amplitude and decoherence time decreased when the tip-substrate separation decreased (Fig. 3A), suggesting a stronger coupling of the H_2 molecule with the junction environment. The variation in the tip-substrate separation across the Cu_2N lattice was only ~0.03 Å, as measured from the line cut in fig. S6F. This height variation contributed ~0.006 THz to the frequency shift observed in Fig. 2B.

To provide further insight into the change in the energy separation of the TLS, we varied the sample bias while monitoring the coherent oscillations (Fig. 3, C and D). The oscillation frequency increased by ~0.2 THz upon changing the sample bias from −50 mV to 40 mV (Fig. 3E). The total electric field experienced by the H_2 molecule trapped in the STM cavity was a combination of the surface electrostatic field and the DC field from the sample bias. As we altered the sample bias without changing the tip position or tip-substrate separation, the

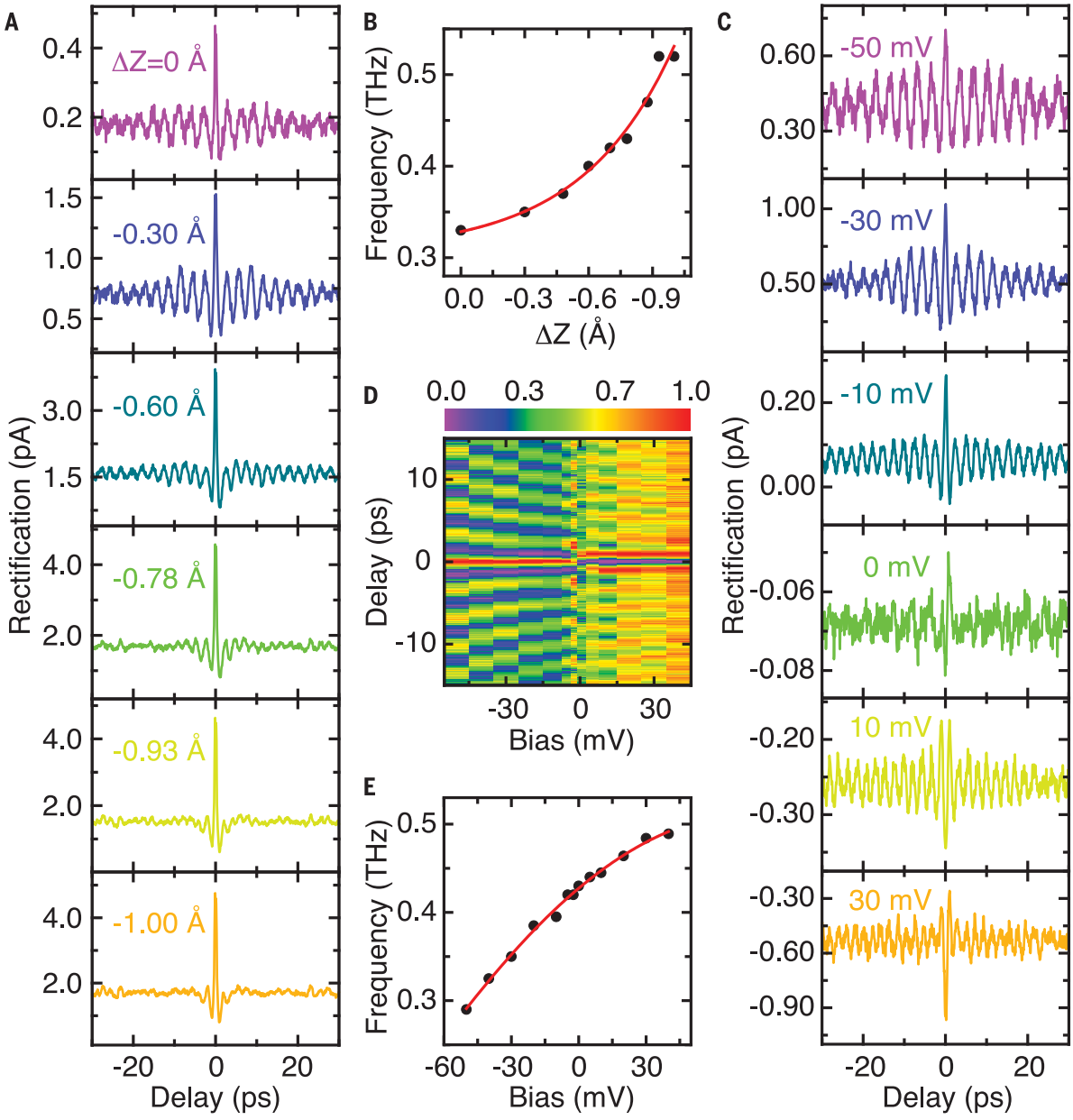

Fig. 3. Coherent oscillation dependency on tip-substrate separation and sample bias. (**A**) THz pump-probe measurements at various tip-substrate separations. The separation is controlled by ramping the tunneling current before turning the feedback off at −20 mV. The bias is then ramped to −30 mV to take the measurements. The colored texts label the corresponding change of tip-substrate separation. (**B**) Oscillation frequency at each change of tip-surface separation from FFT of the time domain measurements in (A); the red line is an exponential fit. (**C**) THz pump-probe measurements at various sample biases. The sample bias is controlled by ramping the bias after turning the feedback off at −20 mV/40 pA. The colored texts label the corresponding sample bias. (**D**) Color map of a series of THz pump-probe measurements, some of which are displayed in (C); the change of the coherent oscillation as a function of sample bias can be visualized. For clarity, the intensity of all of the spectra is normalized positively to the color palette with range (0, 1). (**E**) Oscillation frequency at each bias from FFT of the time domain measurements in (C); the red line is a fitting of the data with function described in the supplementary materials.

DC field varied while the surface electrostatic field remained the same. Because the energy levels shifted under external field through the Stark effect, the energy separation of the TLS changed. Analysis and fitting of the data in Fig. 3E yielded a surface electrostatic field of 43 mV/Å pointing toward the surface. In addition, the dipole moment difference of the two states along this field was extracted and found to be ~0.6 debye. Details of the fitting are described in the supplementary materials. Besides varying the sample bias, the coherent oscillation frequency could also be shifted for different tips under the same sample bias (fig. S12). Effectively, the DC fields varied with tip structure from different tips, which modified the total electric field acting on the H_2 and thus changed its oscillation frequency.

We acquired THz rectification images in real space with atomic-scale spatial and femtosecond-scale temporal resolutions. The spectroscopic features of the TLS exhibited temporal evolution that sensitively depended on the molecule's surrounding environment in the surface plane. As shown in Fig. 4, a series of constant-height THz rectification imaging was recorded at different time delays between pump-probe

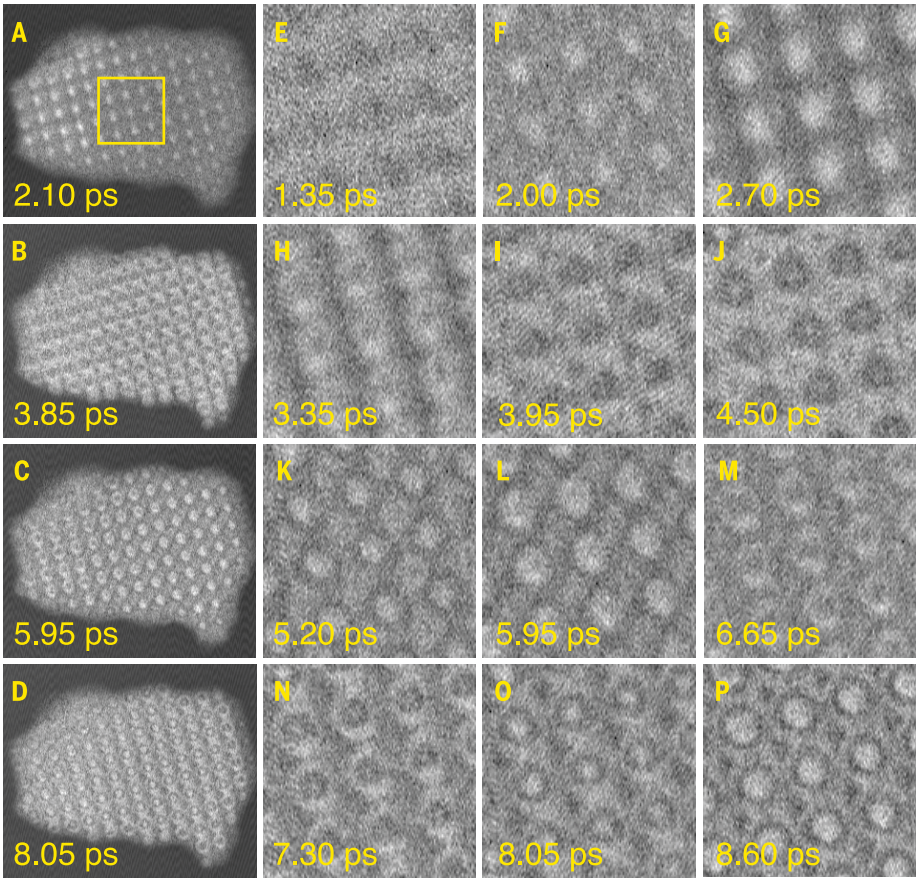

Fig. 4. Temporal snapshots of THz rectification imaging of Cu_2N surface at various delay times. (**A** to **D**) Rectification imaging of the entire Cu_2N island at four different delays. For each pixel in the images, tip is positioned at setpoint −20 mV/40 pA, and then feedback is turned off and bias is ramped to −30 mV. Feedback is turned on before and during the tip movement to the next pixel. All images are 53.2 Å × 44.9 Å and 266 × 224 pixels. (**E** to **P**) Series of zoom-in rectification images at various delays. All images are 13.8 Å × 13.8 Å and 137 × 137 pixels.

pulses. These images provided temporal snapshots of the spatial variations of the H_2 TLS coherence caused by the heterogeneity of the surface. Four successive images of the whole Cu_2N island (Fig. 4, A to D) revealed the wavelike evolution of the "ripples" from the upper left to the bottom right of the island.

A series of images (Fig. 4, E to P) of the yellow square window in Fig. 4A revealed the alternation of the ripple features between bright and dark, or high and low rectification current, as a function of the time delay. Two sequences of temporal snapshots were composed (movies S1 and S2). The properties of the coherent oscillations were highly sensitive to the lateral position of the STM tip (Fig. 2 and fig. S8). In rectification imaging at a chosen delay, the tip was located over different positions of the surface. The oscillation frequency shifted spatially because the surface chemical environment experienced by the H_2 TLS varies over different positions of the surface. The decoherence time also changed as a response to the local environment sensed by the H_2. As a result, the spatially resolved rectification imaging at different delay times effectively revealed the surface chemical environment distribution of the Cu_2N island.

The extreme sensitivity of the H_2 TLS coherent oscillation to the applied electric field and the underlying surface chemical environment heralds the application of the H_2 molecule in the STM cavity for extreme quantum sensing. Relative to other quantum sensors such as NV centers in diamond, the H_2 coherent sensor in the STM cavity provides simultaneous atomic-scale spatial and femtosecond temporal resolutions with GHz energy discrimination. H_2 molecules have been found to be trapped over a variety of surfaces, atoms, and molecules (*22*, *24*, *27*). THz pump-probe measurements with a H_2 molecule in the STM cavity can be used to probe the electrostatic field and potential energy surface of the sample. The ability to measure and control coherent oscillations of the H_2 TLS in different environments opens a route for quantum sensing of a broad range of systems, from single atoms to heteroatomic molecules and solid surfaces.

REFERENCES AND NOTES

1. C. L. Degen, F. Reinhard, P. Cappellaro, *Rev. Mod. Phys.* **89**, 035002 (2017).
2. F. Troiani, A. Ghirri, M. G. A. Paris, C. Bonizzoni, M. Affronte, *J. Magn. Magn. Mater.* **491**, 165534 (2019).
3. M. S. Grinolds *et al.*, *Nat. Phys.* **7**, 687–692 (2011).
4. N. Aslam *et al.*, *Science* **357**, 67–71 (2017).
5. P. Maletinsky *et al.*, *Nat. Nanotechnol.* **7**, 320–324 (2012).
6. K. Bian *et al.*, *Nat. Commun.* **12**, 2457 (2021).
7. M. J. Biercuk, H. Uys, J. W. Britton, A. P. VanDevender, J. J. Bollinger, *Nat. Nanotechnol.* **5**, 646–650 (2010).
8. M. J. Yoo *et al.*, *Science* **276**, 579–582 (1997).
9. J. Martin *et al.*, *Nat. Phys.* **4**, 144–148 (2008).
10. G. Czap *et al.*, *Science* **364**, 670–673 (2019).
11. C. Wagner *et al.*, *Nat. Mater.* **18**, 853–859 (2019).
12. X. Zhang *et al.*, *Nat. Chem.* **14**, 59–65 (2022).
13. P. Willke *et al.*, *Sci. Adv.* **4**, eaaq1543 (2018).
14. T. Choi *et al.*, *Nat. Nanotechnol.* **12**, 420–424 (2017).
15. K. Yang *et al.*, *Science* **366**, 509–512 (2019).
16. S. Baumann *et al.*, *Science* **350**, 417–420 (2015).
17. T. L. Cocker, D. Peller, P. Yu, J. Repp, R. Huber, *Nature* **539**, 263–267 (2016).
18. S. Li, S. Chen, J. Li, R. Wu, W. Ho, *Phys. Rev. Lett.* **119**, 176002 (2017).
19. D. Peller *et al.*, *Nature* **585**, 58–62 (2020).
20. N. T. Yardimci, S. H. Yang, C. W. Berry, M. Jarrahi, *IEEE Trans. Terahertz Sci. Technol.* **5**, 223–229 (2015).
21. J. A. Gupta, C. P. Lutz, A. J. Heinrich, D. M. Eigler, *Phys. Rev. B* **71**, 115416 (2005).
22. S. Liu, A. Shiotari, D. Baugh, M. Wolf, T. Kumagai, *Phys. Rev. B* **97**, 195417 (2018).
23. P. Chen, Z. Xiong, J. Luo, J. Lin, K. L. Tan, *Nature* **420**, 302–304 (2002).
24. F. D. Natterer, F. Patthey, H. Brune, *ACS Nano* **8**, 7099–7105 (2014).
25. F. D. Natterer, F. Patthey, H. Brune, *Phys. Rev. Lett.* **111**, 175303 (2013).
26. S. Li *et al.*, *Phys. Rev. Lett.* **111**, 146102 (2013).
27. S. Li *et al.*, *Phys. Rev. Lett.* **114**, 206101 (2015).
28. J. Jung, S. Nam, C. Wolf, A. J. Heinrich, J. Chae, *RSC Adv.* **11**, 6240–6245 (2021).
29. A. Halbritter, P. Makk, S. Csonka, G. Mihály, *Phys. Rev. B* **77**, 075402 (2008).
30. W. H. A. Thijssen, D. Djukic, A. F. Otte, R. H. Bremmer, J. M. van Ruitenbeek, *Phys. Rev. Lett.* **97**, 226806 (2006).
31. H. Wang *et al.*, *J. Phys. Chem. Lett.* **6**, 3453–3457 (2015).
32. T. Choi, C. D. Ruggiero, J. A. Gupta, *Phys. Rev. B* **78**, 035430 (2008).
33. C. F. Hirjibehedin *et al.*, *Science* **317**, 1199–1203 (2007).
34. J. Lee, X. Tu, W. Ho, *Nano Lett.* **5**, 2613–2617 (2005).
35. X. W. Tu, J. H. Lee, W. Ho, *J. Chem. Phys.* **124**, 021105 (2006).
36. M. Schneiderbauer, M. Emmrich, A. J. Weymouth, F. J. Giessibl, *Phys. Rev. Lett.* **112**, 166102 (2014).
37. K. T. Crampton, J. Lee, V. A. Apkarian, *ACS Nano* **13**, 6363–6371 (2019).

ACKNOWLEDGMENTS

The plasmonic photoconductive antenna was fabricated by M. Jarrahi's group at the University of California, Los Angeles. **Funding:** Supported by US Department of Energy, Office of Basic Energy Sciences, award DE-SC0019448. **Author contributions:** Experiment, analyses, and manuscript preparation were jointly carried out by L.W., Y.X., and W.H. **Competing interests:** The authors declare no competing interests. **Data and materials availability:** All the data are available in the main text and the supplementary materials.

SUPPLEMENTARY MATERIALS

science.org/doi/10.1126/science.abn9220
Materials and Methods
Figs. S1 to S12
Movies S1 and S2

30 December 2021; resubmitted 11 February 2022
Accepted 25 March 2022
10.1126/science.abn9220

Atomic-scale quantum sensing based on the ultrafast coherence of an H molecule in an STM cavity

Likun WangYunpeng XiaW. Ho

Science, 376 (6591), • DOI: 10.1126/science.abn9220

Spatial sensing with hydrogen

The coupling of coherent quantum systems to the surrounding environment can be used to create highly sensitive sensors, but many surface-based implementations, such as nitrogen vacancies in diamond, have limited spatial resolution. Wang *et al*. created a quantum sensor with high spatial sensitivity by using the electric field from a scanning tunneling microscope tip to confine a hydrogen molecule on copper nitride islands grown on a copper surface. Femtosecond-pulse terahertz spectroscopy was used to follow the coherence of the two-level system created by different adsorption geometries. The temporal oscillations and decoherence in the superposition state showed spatial variations at the sub-angstrom scale. —PDS